ROTOR DYNAMICS OF MODERN TURBOCHARGERS

Tomáš Fryščok[1]

Summary: Target of this article is to determine eigenvalues of the rotating parts of TC by series of measurement and subsequently to compare them with the predicted data from calculating software. The data were measured at the compressor side on a special compressor nut which is used especially for shaft motion measurement. The TC was installed on the internal combustion engine. The measurement was done within several loads and increasing oil inlet pressures and temperatures.

Key words: Semi floating ring bearing (SFRB), shaft motion (SM), rotor dynamics, eigenvalues, fast Fourier transform FFT, Turbocharger (TC)

INTRODUCTION

This work shows the differences between predicted and real measured data of linear and nonlinear rotor dynamic models. This type of TC is designed for passenger cars and uses a semi floating ring bearing. The waterfall spectra of rotor assembly were measured at the compressor nose. The rotor depicts a complex response, it means synchronous (shaft rotating speed), sub synchronous and super synchronous frequencies which are observed at high TC speed. Post processing of the test data has been performed by mathematical software, which allows filtering the synchronous, sub synchronous and super synchronous vibration components for later comparisons to the predicted shaft motions. The static performance of the semi floating ring bearings has been analyzed with provided software, which is able to predict the motion of the shaft and bearing components as well as static loading on the bearing due to lubricant feed pressure and incoming lubricant temperature. In addition, the program calculates rotor dynamic force coefficients for the inner and outer films of the semi floating ring bearing. The turbocharger model for the linear and nonlinear analyses includes lumped masses for the compressor and turbine wheels and the thrust spacer. The mass imbalance distribution on the TC rotor is estimated from the test data using a procedure derived from the two-plane balancing method with influence coefficients.

The linear model yields predictions of rotor synchronous response to imbalance and damped eigenvalues. The analysis evidences that the rotor cylindrical-bending mode is unstable at all shaft speeds while the rotor conical model becomes more unstable as lubricant feed pressure decreases. The linear stability results predict two critical speeds occurring at 45 000 and 131000 rpm. The first critical speed corresponds to the rotor cylindrical-bending mode. The second critical speed connected to the rotor first bending mode. In the nonlinear transient analysis, the nonlinear equations of motion of the system (rotor-SFRB) are

[1] Ing. Tomáš Fryščok Brno University of Technology, Faculty of Mechanical Engineering, Institute of Automotive Engineering, Technická 2896/2, 616 69, Brno, Czech Republic, Tel +420739353726, Fax +420541143 939 E-mail: tomasfrycok@seznam.cz

integrated, and the bearing reaction forces are calculated at each time step in a numerical addition procedure. The model then yields predictions of total motion which is decaying into synchronous and sub synchronous motion, amplitudes and frequencies. The nonlinear analysis predicts synchronous amplitudes that associate quite good with the test data at higher shaft speeds.

1. EXPERIMENTAL

1.1 Prediction of test turbocharger

This section describes the structural model of the above mentioned TC using the rotor dynamic software. The properties of the rotor assembly are used to create a lumped model to predict linear and nonlinear response of the rotor bearing system. Measurement of the rotor free-free mode and natural frequencies are performed in order to confirm the rotor dynamic model. Then stiffness and damping of the SFRB for a definite static load are predicted.

The analysis of the SFRB is significant for the study of dynamics of the rotor-bearing system, mass of inertia and place where imbalances are situated. For this reason, it is necessary to create the model properly. This modeling is based on the influence coefficient method for balancing a rotor.

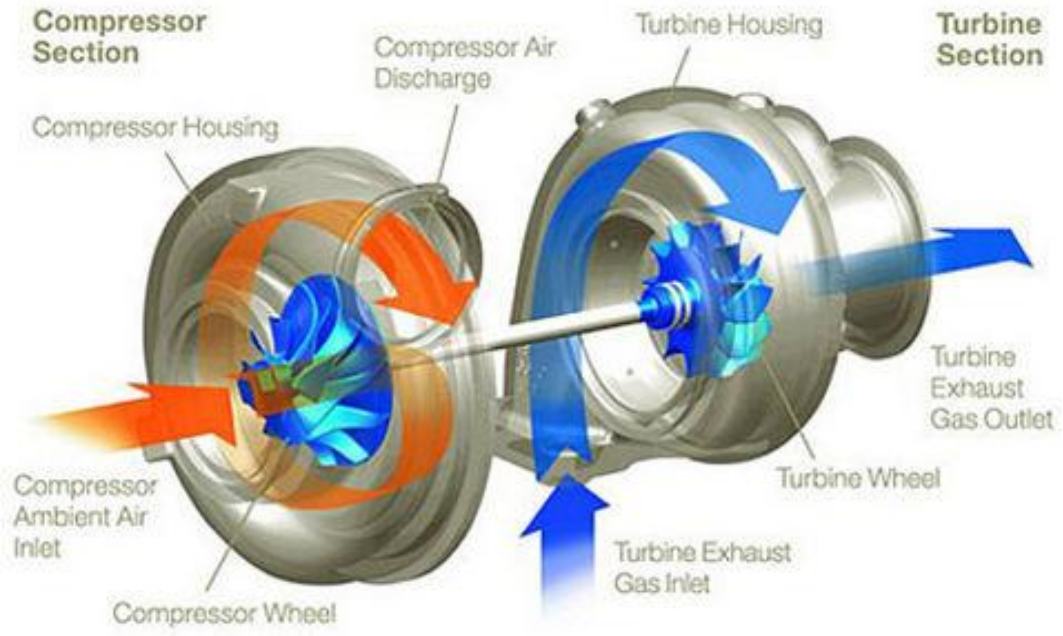

Source: http://jalopnik.com/turbocharger/

Fig. 1 - Turbocharger structural model

1.2 Model of rotor bearing system

Fig. 1 shows a TC structural model including details of rotating parts. A semi-floating ring bearing (SFRB) supports the rotor at two locations near the turbine and compressor wheels. Fig. 2 shows a model of TC rotor for computing software. This model includes lumped masses for the compressor and turbine wheels and the thrust spacer; is composed of 55 finite elements (50 stations) of the rotor, compressor and turbine wheel, and one fixed ring bearing (yellow color). The spring connections represent a fluid film bearing. It should be

noted that only the outer fluid films can be seen in the graph below. Inner film connections cannot be distinguished due to their small clearance.

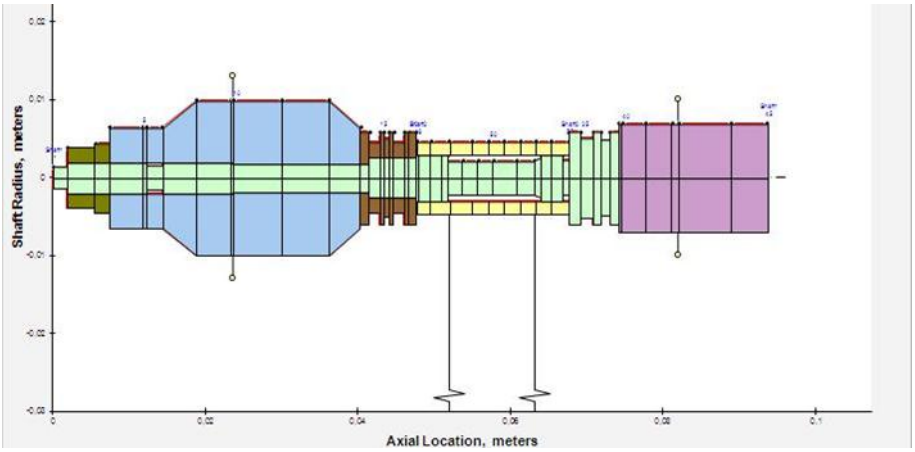

Source: Author

Fig. 2 - Model of rotating assembly for calculating software

The rotor dynamic model includes imbalance masses located on the compressor and turbine wheels. Values as weight, moment of inertia and polar moment of shaft thrust spacer; compressor and turbine wheel were calculated in Catia software. The illustrations of each rotating part can be seen in Fig. 3 - 5 below.

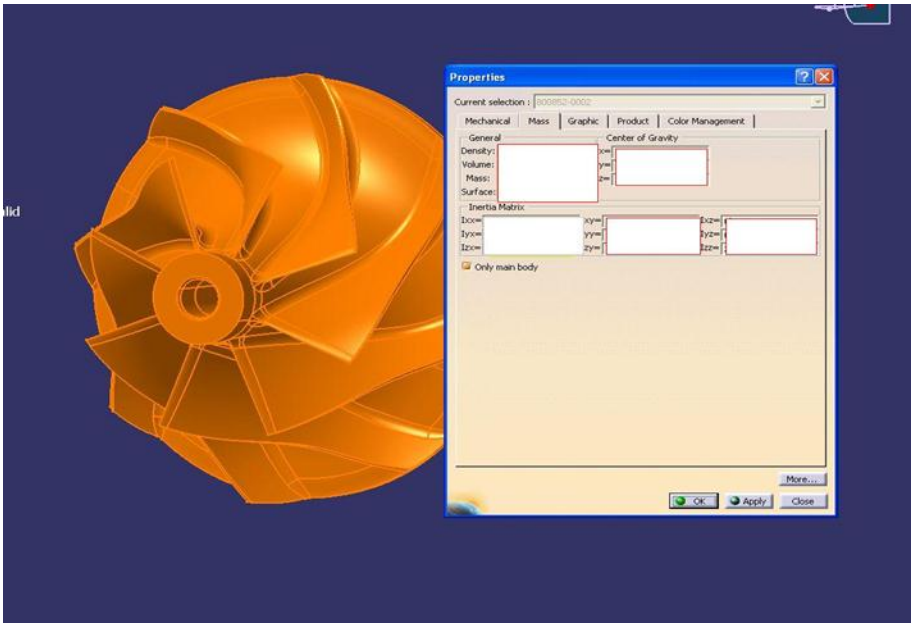

Source: Author

Fig. 3- 3D model of compressor wheel

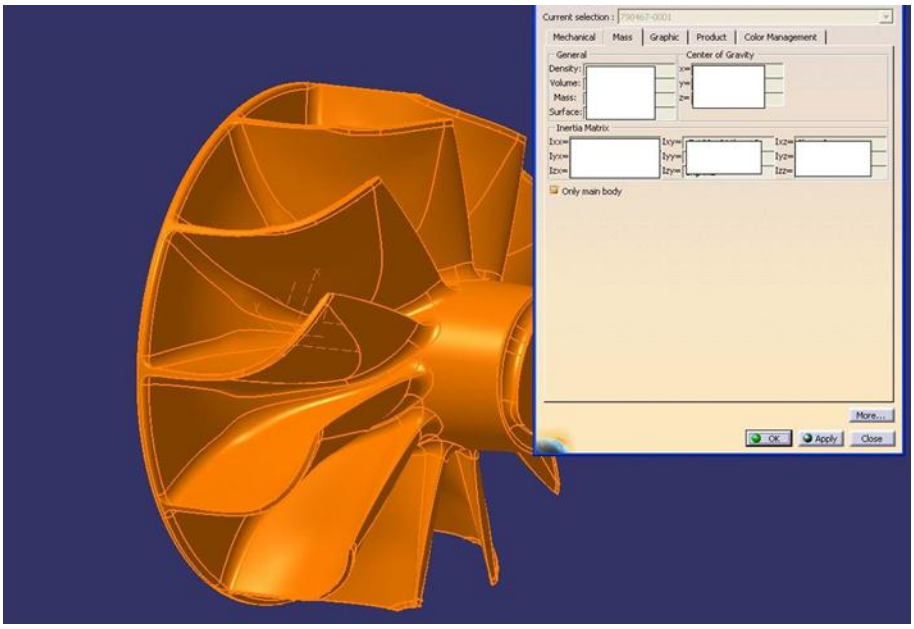

Source: Author

Fig. 4 - 3D model of turbine wheel

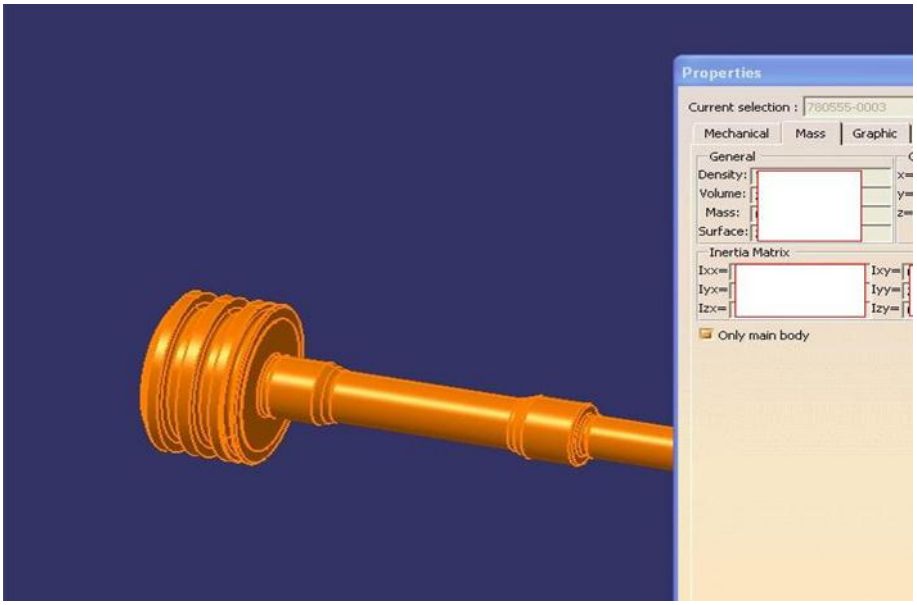

Source: Author

Fig. 5 - 3D model of shaft

Free-free mode shapes and natural frequencies of a rotor distinguish the response of the rotor in the absence of any support and in the absence of rotation. A good correlation between experimental and predicted values is essential to validate the rotor dynamic model.

1.3 Governing equation of motion

Governing equations (1, 2) for the used rotor bearing system, in steady state regime with constant speed Ω, are as follows

$$M\ddot{y}(t) + (C_b + \Omega G)\dot{y}(t) + (K_s + K_b) + y(t) = Q(\dot{y}, y, \Omega, t) \quad (1)$$

The above equations can be simplified into the form

$$M\ddot{y}(t) + C\dot{y}(t) + Ky(t) = Q(\dot{y}, y, \Omega, t) \quad (2)$$

The y letter represents the displacement vector. The mass (inertia) matrix commonly marked by M and it is a positive definite real symmetric matrix. G represents real skew-symmetric matrix it is a significant part of the rotational kinetic energy caused by the gyroscopic moments. The letter K_s means structural stiffness matrix comes from strain energy. The matrix C_b is a linearized bearing dynamic damping and K_b means linearized bearing stiffness matrix. These equations are non-symmetric real matrices, due to the reality that bearings are nonconservative in nature. Forcing vector is represent by letter Q and include all the forcing functions like synchronous excitation (rotor assembly has always some residual unbalance) disk skew, shaft bow, static load and constant gravity.

It should be mentioned here also the second equation of motion, is used to study the rotor motion during the startup, shutdown phase and transition thought critical speed. This equation is characterized by angular velocity. Spin speed is not constant and is a function of time (t).The equation of motion for different rotational speed systems is

$$M\ddot{y}(t) + [C_b + \dot{\varphi}G]\dot{y}(t) + \left[(K_s + K_b) + \ddot{\varphi}G\right]y(t) = \varphi^2 Q_1(\varphi) + \ddot{\varphi}Q_2(\varphi) + Q_3(\dot{y}, y, \varphi, \dot{\varphi}, \ddot{\varphi}, t) \quad (3)$$

Lettersφ, $\dot{\varphi}$ and $\ddot{\varphi}$ means the output data are stored in time domain form and the analysis is performed in the frequency area. For transferring the data to the frequency domain, FFT was used. The size of the time increment Δt specifies the number of data points and a sampling frequency (4). The number of data points was given by equation (5), angular displacement, angular velocity ($\dot{\varphi} = \Omega$) and angular acceleration or deceleration of the rotor system. This equation introduces due to various speeds two new parameters, which are: circulatory matrix $\ddot{\varphi}G$ and forcing function$\ddot{\varphi}Q_2$. Next section discusses about fast Fourier transform.

1.4 Fast Fourier transform

The output data are stored in time domain form and the analysis is performed in the frequency area. For transferring the data to the frequency domain, FFT was used. The size of the time increment Δt specifies the number of data points and a sampling frequency (4). The number of data points was given by equation (5).

Sampling frequency

$$\mathrm{Fs} = \frac{1}{\Delta \mathrm{t}} \quad (4)$$

$$n = \frac{(t_f - t_i)}{\Delta \mathrm{t}} + 1 = \frac{ending\ time - starting\ time}{increment} + 1 \quad (5)$$

The rule for FFT algorithm requires the number of data points to be of (N) power of 2 (N≤ n). FFT calculates discrete periodic waveforms (frequency harmonics) which sum up the

original time domain signal. The range of frequencies in FFT is from 0 (DC signal) to Fs/2 (the Nyquist frequency which is equal to maximum frequency in the spectrum).

1.5 Rotor steady state transient motion

A lateral motion is monitored by two orthogonal proximity probes positioned orthogonally. There is a phase shift between X and Y; probes produce voltage proportional to the distance between the shaft and sensor. In this case the reference value is taken from the rotor start position. The orbits (steady state lateral motion) are generated from two time sine waves in X and Y, time direction is eliminated and remains only the dependence between X and Y amplitudes shown in Cartesian coordinate. The X and Y have the same frequency, but different amplitude and phase shift. The simple expression can represent a steady state synchronous response with whirl frequency. The simplest equations of steady state rotor motion are given below

$$x(t) = x_c cos\omega t + x_s sin\omega t = |x|\cos(\omega t - \varphi_s) \quad (6)$$

$$y(t) = y_c cos\omega t + y_s sin\omega t = |y|\cos(\omega t - \varphi_s) \quad (7)$$

where

$$|x| = \frac{me\Omega^2}{\lfloor (K_x - \Omega^2 m)^2 + (\Omega C_x)^2 \rfloor^{1/2}} \quad (8)$$

$$\varphi_x = arctan\left(\frac{(\Omega C_x)}{K_x - \Omega^2 m}\right) \quad (9)$$

$$|y| \frac{me\Omega^2}{\left\lfloor (K_y - \Omega^2 m)^2 + (\Omega C_y)^2 \right\rfloor^{1/2}} \quad (10)$$

$$\phi_y = arctan\left(\frac{K_y - \Omega^2 m}{-\Omega C_y}\right) \quad (11)$$

1.6 Experimental Whirl speed map

The experimental whirl speed map is a plot of damped natural frequencies (whirl speeds), of rotor system versus rotor spin speed. Rotor rotational speed is along the X axis. The rotor whirl frequency is along the Y axis. The damped critical speeds and any excitation resonance speeds are determined by noting the coincidence of the shaft speed with the system natural frequencies for a given excitation frequency line ($\omega_{ext} = \alpha\Omega$) in the whirl speed map. The value which is equal to one in the excitation slope is coupled with the synchronous excitation that is the main interest. The rotating unbalance always exists (there is always a residual imbalance). In this case of rotor system, the translational motion will be solved by Laval-Jeffcott rotor; the natural frequencies are independent of the spin speed.

1.7 Experimental modal analysis

The experimental modal analysis has a great importance in technical diagnostics. This method can provide a complete technical description of mechanical system or measured structure. Outputs from EMA are damped natural frequency and mode shapes. Predicted data calculated by software are verified by measured values from EMA. In the experiment, above mentioned values from frequency response are obtained by using FFT.

The essence is the time domain response during the dynamic excitation (impact modal hammer or shaker) of measured system which is a rotor assembly in this case. The result is a dynamic compliance system. This function is defined as

$$H(\varpi) = \frac{X(\varpi)}{F(\varpi)} \quad (12)$$

Displacement or acceleration measurements are always observed in a real system at damped vibrations, where deflection of final value will always correspond to resonance frequency. The results of experiment need to be in frequency domain due to discretization of problem component etc. FFT will be used for change from time domain to frequency domain. The goal of this measurement is a simple verification of predicted eigenvalues from software.

2. RESULTS

The measurements were performed on the combustion engine designed for passenger cars. This measurement was based on two capacitive proximity probes set up in two planes rotated against to each other by 90 degree. The Nyquist frequency was set up on 25 600Hz. Probes were previously calibrated on calibration equipment, and data were processed by the program created in Labview.

The output data from measurement were transferred by FFT to frequency domain from X and Y probes. Time transient data with maximum whirl diameter and whirl frequency diagram are known as Waterfall. This measuring was performed in a wide range oil inlet temperature and pressures. Oil temperature started at ambient temperature and increased to the maximal temperature above 130 °C; the same was done with different inlet oil pressures from 0.5 up to 3 bars. The aim was to create a map with the influence of pressure and temperature on the measurement results.

Figures below show the frequency response at 750 Hz (45 000 rpm) in X and Y axis directions with 0.5 bar inlet oil and oil temperature 80°C. Kinetic energy was generated by combustion engine at idle regime for both directions. The whole measurement was carried out in the Labview software.

Fig. 6 and 7 illustrate completely processed data achieved at 750 Hz. The first two figures show the processed data with these parameters 100°C and 0.5 bar at oil inlet. The engine was running at a 1500 rpm with a low load.

Fig. 8 and 9 are characterized by lower oil inlet temperature (temperature was consistent with the ambient temperature about 22 °C). These figures display a decreased motion of shaft at compressor nose. The actual value for this temperature is in X axis 0.01779 mm compared to the original (in operating temperature); there is a 0.003 mm difference. Y axis has also noticeable change at first glance. The difference in this direction is 0.00283 mm.

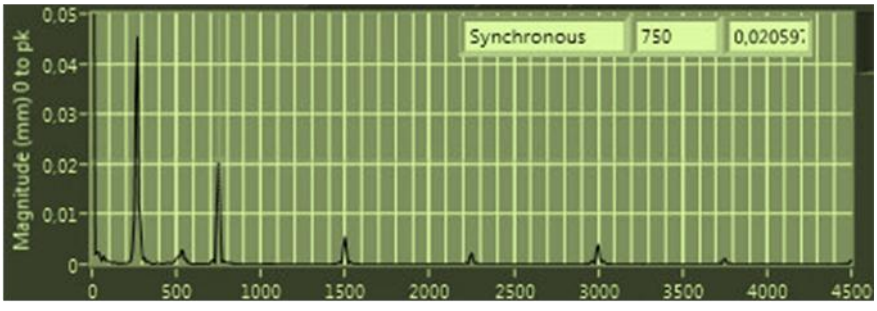

Source: Author

Fig. 6 - FFT analysis for X direction at 750 Hz (oil inlet pressure 2 bar, temperature 80 °C)

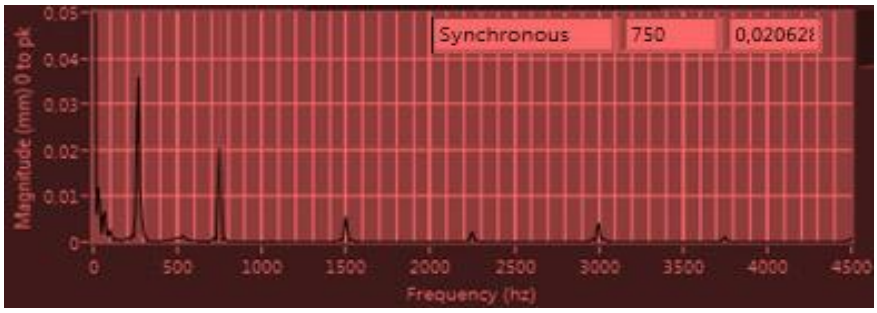

Source: Author

Fig. 7 - FFT analysis for Y direction at 750 Hz (oil inlet pressure 2 bar, temperature 80 °C)

Figures above display quite high sub synchronous (whirling speed) vibration and super synchronous (higher harmonic order) as well. The sub synchronous frequency has almost twice value compared to synchronous frequency.

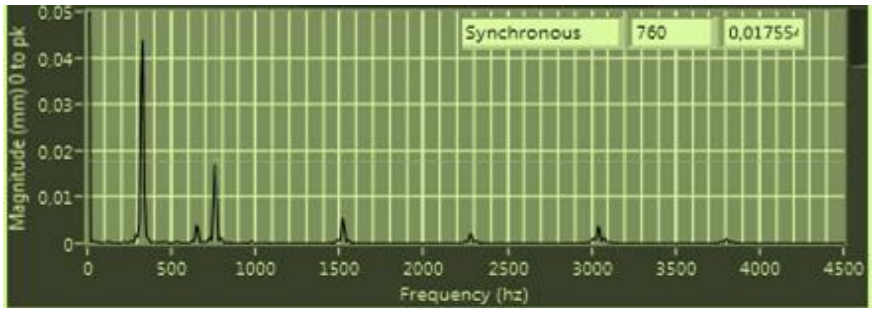

Source: Author

Fig. 8 - FFT analysis for X direction at 750 Hz (oil inlet pressure 2 bar, oil room temperature)

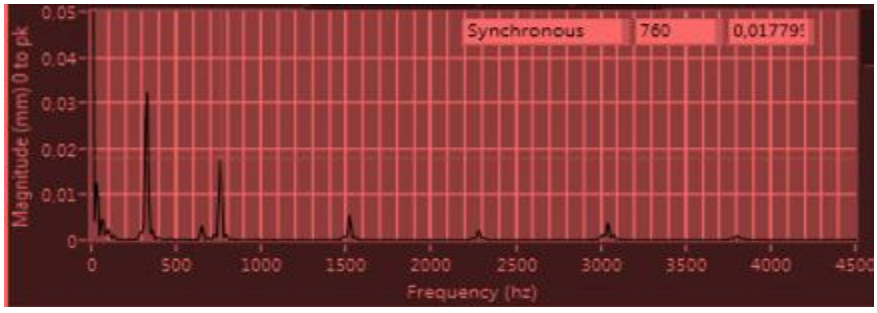

Source: Author

Fig. 9 - FFT analysis for Y direction at 750 Hz (oil inlet pressure 2 bar, oil room temperature)

Fig. 10 indicates the motion of rotor system depending on time the sampling frequency for this measurement was set to 25 600Hz. The whirl speed map was measured from the ramp-up and coast-down regime. The imaginary center of shaft is out of axis center system. The possible reasons are low rotor speed (low hydrodynamic force) and center of shaft was not set up at the zero positions or load generated from engine. The whirl frequency diameter in this case is 0.165mm.

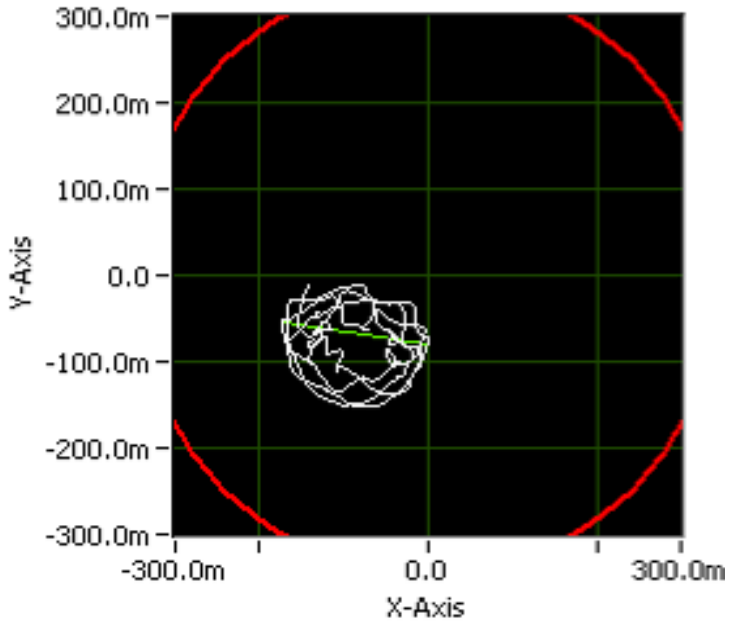

Source: Author

Fig. 10 - Rotor time transient motion

The whirl speed map was measured during the ramp-up phase with a 50Hz increment and the same measurement was performed in the opposite coast-down direction. In Fig. 11 below is shown cascade diagram for X direction, the measured data for Y direction is illustrated in Fig. 12. There are visible two critical frequencies. The axis values are eliminated due to laboratory request. In the figure are clearly visible two sub synchronous whirl speeds.

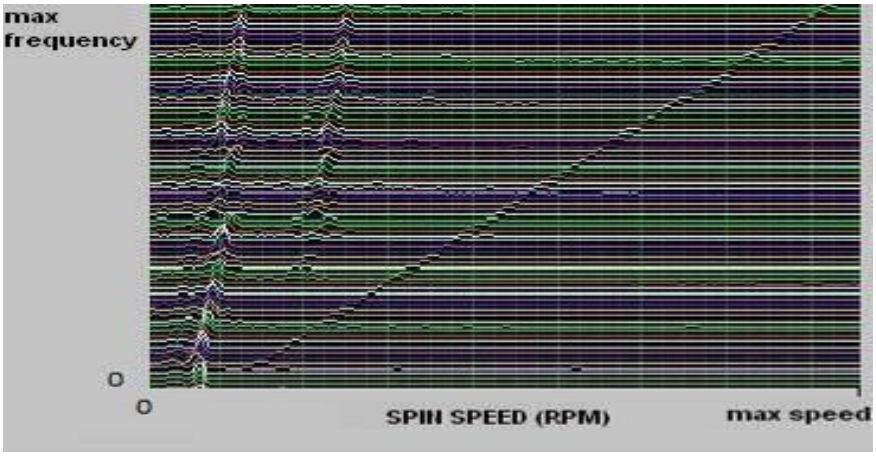

Source: Author

Fig. 11 - Whirl speed map in X axis direction

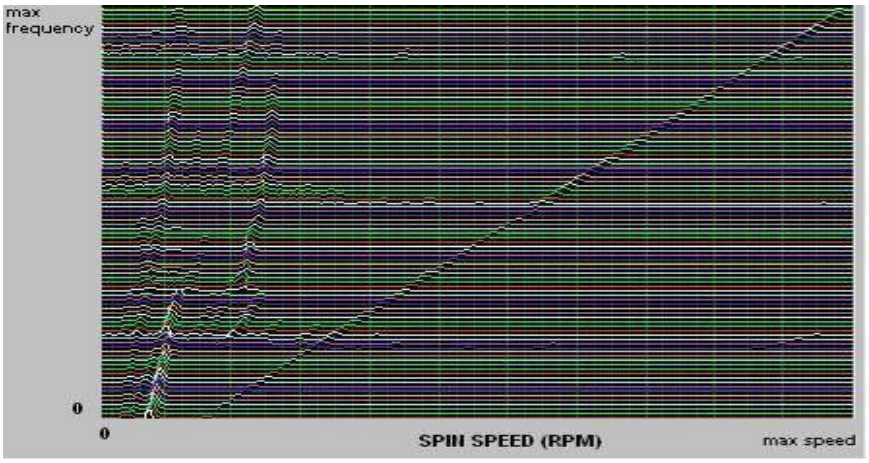

Source: Author

Fig. 12 - Whirl speed map in Y axis direction

Results from experimental modal analysis are shown in Fig. 13. The excitations were performing by impact hammer with different weights to achieve excitation whole frequency range. The rotor assembly was tested by EMA, which was attached freely on elastic cord cables to reduce influence of eigenvalues on remaining turbocharger parts. Figure below shows two natural frequencies, the first is close to 750 Hz and the second natural frequency is more damped (lower peak) and occur at 2000 Hz. On left sides of Figure are data recorded in time domain and on the right side are data in frequency domain processed by FFT transformation.

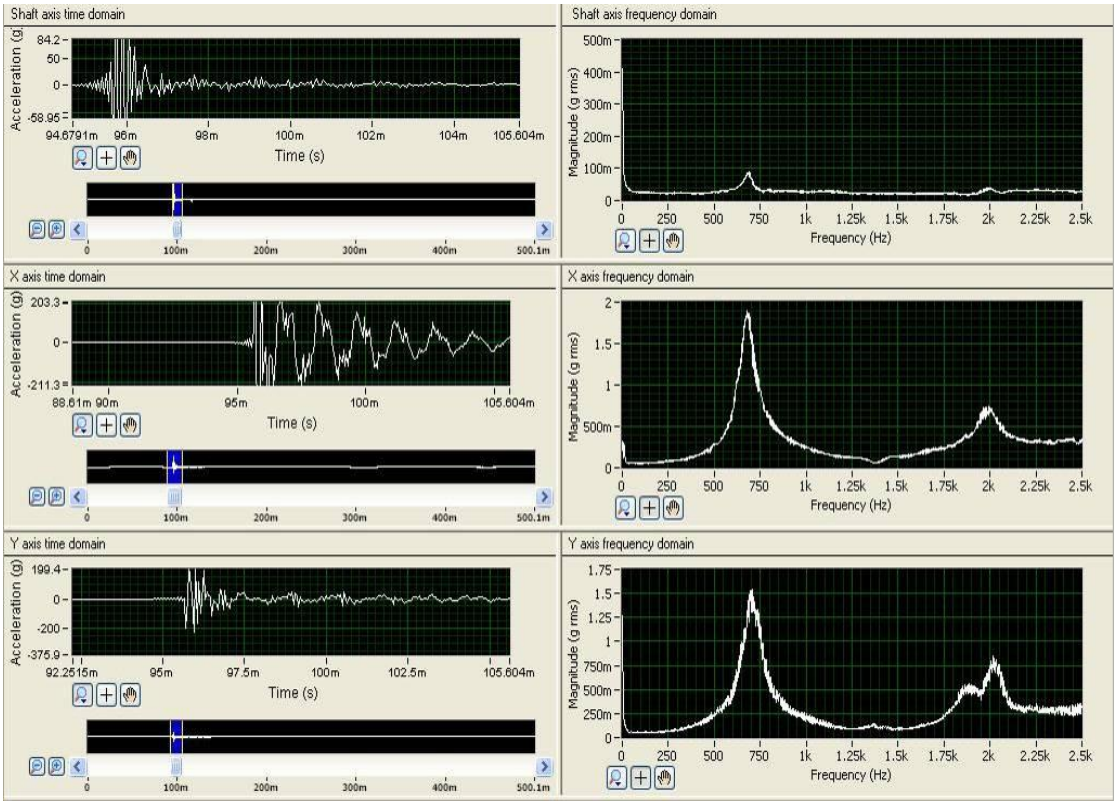

Source: Author

Fig. 13 - Experimental modal analysis of rotor assembly (shaft, turbine and compressor wheel)

CONCLUSION

In the article were performed mathematical calculations of eigenvalues (critical speeds of rotating parts, predicted of Campbell diagram. Weight and moment were calculated in Catia software of for all rotational parts, there have been added also information about system unbalance. Based on these inputs, were calculated critical speeds, damping and stiffness coefficients, whirl speed frequency. This measuring was performed in wide range oil inlet temperature and pressures.

Experimental was dedicated to the actual measurement which was performed on combustion engine for passenger cars. The results from measurement were described in detail at previous chapters began with FFT and end by experimental rotor whirl motion.

The measured data were processed by the program created in Labview. In the article was presented completely processed the data at 750Hz. In this speed are processed FFT in both planes; rotor time transient motion and measured data was seen at Campbell diagram (Cascade chart) as well. Some data was corrected for presentation in this article due to laboratory request.

Cascade diagram above show quite good correlation between experiment and predicted data, the difference between predicted and measured value are lower than 10% for first predicted critical speed. The differentiation between real a prediction data for second critical speed is close to difference for first critical speed.

ACKNOWLEDGEMENTS

Published results were acquired with the help of the project Development of New Approaches for Decreasing of Powertrain Vibrations, No. FSI-S-11-8, granted by the specific university research of Brno University of Technology.

REFERENCES

(1) CHEN, W. J., GUNTER, E. J. *Dynamics of rotor-bearing systems*, (2010) ISBN 978-1-4120-5190-3

(2) TŮMA, J. *Zpracování signálů z mechanických systémů užitím FFT*, (1997) ISBN 80-901936-1-7

(3) SCHWARZ, B. J., RICHARDSON, M. H. (1999). *Experimental modal analysis*, Jamestown, California 95327

(4) EHRICH, F. F. *Handbook of rotordynamics*, (2004), Krieger publication

(5) The turbomachinery laboratory, *XLTRC2 Brochure*, Texas A&M University, Tamu 3254

(6) RAO, J.S. *Rotor dynamics Third edition*, (1996), ISBN 81-224-0977-6